Comparative Adsorption of Synthetic Dyes Using Low-Cost Biosorbents: Analysis of Thermodynamics and Isotherms

Belin Jude A[1], Divya P[2], Chaitanya M.S.K[3], Renuka V[4], Vanitha S[5], Sankaran A[6*]

[1]Department of Civil Engineering, Saranathan College of Engineering, Tiruchirappalli, Tamil Nadu 620012, India. (dr.abjude@gmail.com)

[2]Department of Physics, S.A. Engineering College, Chennai, Tamil Nadu 600077, India. (drdivyap@saec.ac.in)

[3]Department of Civil Engineering, S.R.K.R. Engineering College, Bhimavaram, Andhra Pradesh 534204, India. (chaitanya.msk@gmail.com)

[4]Department of Chemical Engineering, St. Joseph's College of Engineering, Chennai, Tamil Nadu 600119, India. (renuka7067@gmail.com)

[5]Department of Civil Engineering, Sathyabama Institute of Science and Technology, Chennai, Tamil Nadu 600119, India. (vanitha.civil@sathyabama.ac.in)

[6*]School of Marine Engineering and Technology, Indian Maritime University, Chennai, Tamil Nadu 600119, India. (sankaran.arumugam@gmail.com)

Corresponding author: Sankaran A email: sankaran.arumugam@gmail.com

GRAPHICAL ABSTRACT
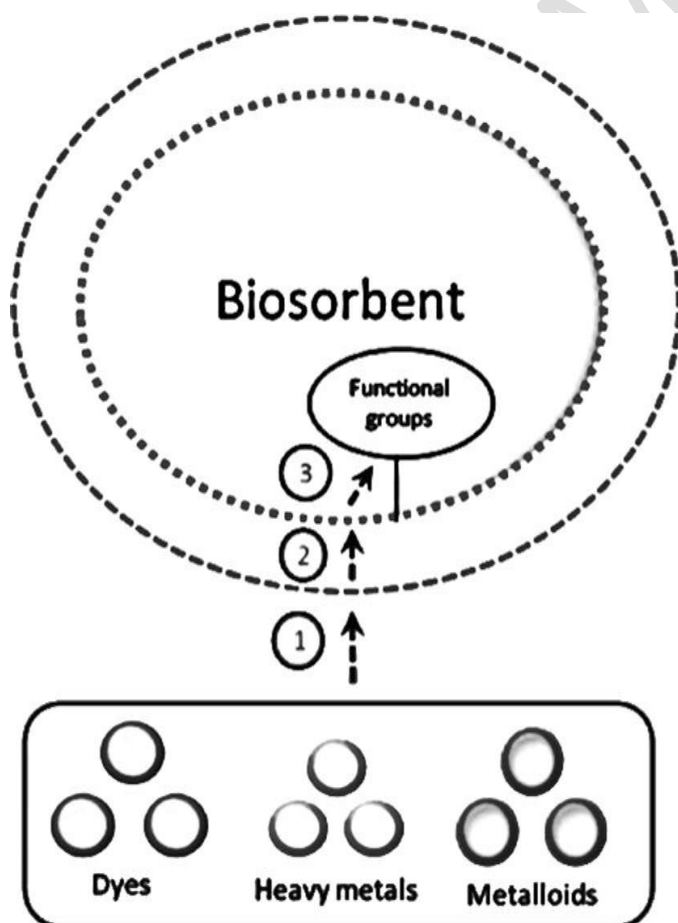
ABSTRACT

The biosorption of azo dyes from the aqueous solutions were investigated using the Prosopis Juliflora Root Powder (PJRP). The experiments involved varying the initial dye concentrations (10 – 50 mg/L), the reaction time of 90 minutes, dye solution's pH level varied from 2.0 to 7.0, and sorbent dosages from 1 to 5 g/20mL. The original dye solution's temperature and ionic strength, among other variables influencing the absorption process, were also investigated. Adsorption isotherms for Temkin, Langmuir, and to replicate the adsorption data, Freundlich was employed. R^2 > 0.95 for CR, CV, and MB, respectively, show that they fit relatively well with the initial state data of the biosorption technique progression. The adsorption kinetics were confirmed using first and second-order pseudo models. The assessment of thermodynamic constants, such as $\Delta G°$, $\Delta H°$, and $\Delta S°$, was carried out. It was discovered that the two dyes had endothermic dye adsorption processes. At an optimal pH, the highest adsorption capacity Q_o for MB was 92.4 mg/g, while for CV, it was 88.9 mg/g, and for CR, it was 82.26 mg/g.

Keywords: Biosorption, Azo dyes, Juliflora roots, Isotherm and Kinetic studies, Thermodynamics.

1. INTRODUCTION

Pollution is intensified by discharging hazardous substances into the environment due to industrial processes, including smelting, mining, manufacturing, and applying metals in agricultural fertilizers and pesticides. In numerous regions, especially in developing countries with weak environmental regulations, sewage that has not been properly treated or is left untreated is often discharged into rivers, lakes, and oceans (Priya et al., 2022). The textile sector influences a significant portion of the economies of many nations worldwide. The wastewater effluents from various sectors, including leather, textiles, and dyestuff, contain a variety of synthetic colours. Dye-containing effluents cause strong colouration and significant water contamination. About 10,000 commercially available dyes with various chemical structures (Abdelmajid et al., 2017). The ionic charge on dye molecules determines whether a dye is anionic, cationic, or non-ionic. Over anionic dyes, cationic dyes are more hazardous. The elimination of artificial industrial dyes is a major environmental problem since most of these dyes and their degradation products can potentially be dangerous and carcinogenic (Achmad et al., 2018). In recent years, eliminating synthetic organic dyes from wastewater has become a significant environmental concern. Since dye effluents are synthetic and mostly contain aromatic compounds that are not biodegradable, it might be challenging to treat them. Several biological, physical, and chemical techniques have been used to treat wastewater containing dyes. Those techniques include membrane separation, sorption, oxidation/ozonation, coagulation/flocculation, and anaerobic/aerobic treatment (Mehrnaz et al., 2020). An efficient approach to removing the colour from wastewater is the adsorption process, one of various chemical and physical procedures. A costly adsorbent, activated carbon has significant

manufacturing costs. Nevertheless, it works well. Because of financial concerns, it can also not handle substantial volumes of wastewater. Numerous natural adsorbents have been investigated for their ability to lower dye concentrations in aqueous solutions (Mohammed et al., 2021). Agricultural leftovers are considered a less expensive natural resource that may be used as adsorbents for artificial dyes.

The powdered root of Prosopis juliflora is an agricultural waste product used to make palm oil. Agricultural waste creates complex materials, mostly composed of cellulose and lignin. Ketones, aldehydes, phenolic hydroxides, ethers, and alcohols are polar functional groups in lignin that can bind substances and increase the sorbent material's affinity for organic molecules (Candelaria et al., 2021). However, it has several beneficial uses. Its wood is used for fuel, charcoal, and construction, and its pods provide fodder for livestock. In environmental applications, Prosopis juliflora roots have gained attention for their potential in adsorbing pollutants, including heavy metals and dyes, from wastewater due to their high surface area and chemical properties. Past studies have demonstrated the effectiveness of using Prosopis juliflora root powder as an adsorbent to remove lead, copper, basic dye, and anionic dye from an aqueous solution (Laxmipriya et al., 2020). Three common dyes that have been demonstrated to damage living things after brief contact are Methylene Blue (MB), Crystal Violet (CV), and Congo Red (CR). The current studies sought to determine how well Prosopis juliflora root powder, an inexpensive and readily available adsorbent, removed MB, CR, and CV azo dyes from aqueous solutions. To maximize the elimination effectiveness, the influences of adsorbent dosage, temperature, ionic strength, pH, beginning dye concentration, and contact duration have all been studied with the adsorption percentage.

2. EXPERIMENTAL METHODS AND MATERIALS

2.1 Preparation of biosorbent and characterization

The powdered Prosopis juliflora (PJRP) powdered root, used as an adsorbent in this investigation, was collected from the Ramanathapuram district, Tamil Nadu. To get particles ranging in size from 50 to 80 μm, the raw roots were repeatedly cleaned using distilled water, dried at 100°C for a whole night, and then crushed and filtered through a series of sieves. In a closed container, the sieved powder was kept dry until needed. Adsorption studies were carried out without any physical or chemical manipulations beforehand. When the PJRP mixed with the dye solution, it ensured that no colour was formed. The functional groups in the materials may be identified structurally and compositionally using FTIR spectroscopy. Using Fourier transform infrared (FTIR) spectra, the PJRP's closest composition was examined. With a KBr disc that held 1% of material that had been finely powdered, the spectra were collected in the 4000–400 cm^{-1} range using a spectroscope (FTIR 2000, PerkinElmer). The combination was utilized for infrared (IR) research

after being squeezed into a KBr wafer under vacuum. The microscopic analysis was conducted to check the adsorbent properties and behaviour.

2.2 Synthetic solution preparation

Analytical grade reagents were used in this study to prepare all the chemicals. The Congo Red (CR), Crystal Violet (CV), and Methylene Blue (MB) dyes were prepared as stock solutions using double-distilled water. Absorbance values at 664 nm and 586 nm were measured before and after each experiment using a spectrophotometer (Nanodrop lite) to calculate the concentrations of CR, CV, and MB. Each dye was added separately, and the results were taken into consideration after three trials.

2.3 Batch adsorption studies

The experiments were done in 100 mL polypropylene bottles at 20ºC using a rotary shaker at 65rpm. To get data on equilibrium, sorption investigations were carried out using the batch approach. A known concentration dye solution in 25 mg/L was combined with 0.05 g of PJRP in each experiment, and the solution was then placed in a 250 mL flask with the appropriate temperature, pH, and concentration. 200 rpm was the continuous speed of the mixture stirred by an electromagnetic stirrer. Each experiment was run twice. Whatman filter paper that had a particle retention size of 11 µm for the filtration process was used in this study. The filtrate underwent treatment with concentrated HNO_3 and was analyzed with an atomic absorption spectrophotometer. Two analyses were conducted to verify precision. The following equation 1 was used to compute the proportion of dye removed after reaching equilibrium and quantify the final dye concentration (C_e):

$$\% \ Dye \ removal = \frac{C_i - C_e}{C_i} \ x \ 100 \tag{1}$$

Ce and Ci are the dye's beginning (mg/L) and ultimate (equilibrium) concentrations. The mass balance was used to determine the quantity of dye adsorbed qe (mg/g) onto PJRP using equation 2.

$$q_e = (C_i - C_e)\frac{V}{W} \tag{2}$$

W is the utilized adsorbent's mass (g), and V is the dye solution's volume (L).

2.4 Evaluation of the PJRP Properties

The biosorbent's morphology was assessed using Scanning Electron Microscopy (SEM) before and after chemical activation. This enabled the visualization of surface alterations, such as increased porosity and texture modifications resulting from the activation process. FTIR spectrometry was used to classify and compare the efficient groups in the biosorbent before and after its interaction with azo dyes. This analysis is crucial for understanding the binding sites and chemical interactions between the biosorbent and the dyes. Additionally, thermal decomposition

UV–visible spectroscopy was employed to analyze all samples to detect and quantify azo dyes. To ensure the reliability of the mercury analysis, the instrument's accuracy was validated by examining a certified reference material from sediment.

2.5 Effect of ionic strength (pH$_{ZPC}$)

The determination of the biosorbent's zero-point charge (pHzpc) was conducted utilizing the solid addition method. This approach elucidates the pH level at which the surface of the biosorbent achieves electrical neutrality. The experiment is instrumental in comprehending the adsorption characteristics of the biosorbent across varying pH conditions. The methodology involved using 0.1 M potassium nitrate (KNO$_3$) as the electrolyte. A 50 ml aliquot of potassium nitrate solution was placed in a 250 ml conical flask, and the initial pH was meticulously adjusted to a range between 2.0 and 10.0. Around 0.1 gm of PJRP was added to the azo dye solution. The solution was shaken for 24 hours at 150 rpm using the rotary shaker to ensure the interface between the adsorbate and metal ions. The metal ion solution's final pH (pHf) was verified after 24 hours. The final and initial pH variations were calculated using the relationship of $\Delta pH = pH_o – pH_f$. A graph was subsequently generated with the initial pH (pH$_o$) plotted on the x-axis and ΔpH on the y-axis. The pH$_{zpc}$ of the PJRP biosorbent was identified at the point where the curve intersects the x-axis, signifying the pH at which the biosorbent surface exhibits a net neutral charge.

2.6 Desorption studies

Following the biosorption of azo dyes under batch conditions, we conducted desorption experiments utilizing sulfuric acid (H$_2$SO$_4$) as the eluting agent. This methodology was employed to evaluate the reusability of both native and chemically modified PJRP biosorbents across successive biosorption-desorption cycles. For the desorption experiment, the biosorbent loaded with azo dyes from the prior biosorption phase was oven-dried and placed in a 250 ml conical flask holding 50 ml of the H$_2$SO$_4$ desorbing solution. The experimental parameters, including contact time and agitation speed, were consistent with those applied during the biosorption phase. Upon completion of the desorption process, the regenerated biosorbent was carefully washed with distilled water to eliminate any residual H$_2$SO$_4$. The cleaned biosorbent was then dried in a hot air oven, preparing it for subsequent biosorption cycles. This procedure was repeated for up to three consecutive biosorption-desorption cycles to evaluate the biosorbent's reusability and capacity to retain efficiency over multiple cycles. Such an assessment is crucial for determining the long-term viability of PJRP as a sustainable biosorbent.

3. RESULTS AND DISCUSSION

3.1 FTIR studies

FTIR was used to identify the functional groups in Prosopis juliflora root powder biomass that play a role in biosorption. FTIR spectra were obtained for the empty and azo dye biomass samples within the 400–4000 cm^{-1} range. This study helps identify the specific functional groups that interact with the dyes during the reaction time. The FT-IR spectra of PJRPs containing CV, CR, and MB, as well as the regular PJRP, can be seen in Fig. 1 in sequential order. The wide bands span from 3526.11 to 3749.66 cm^{-1} in wavelength, as shown in Fig. 1, suggesting the presence of amine (–NH) or bonded hydroxyl (–OH) groups. The peaks appearing at 1717.76 cm^{-1} are thought to originate from the stretching vibration of carbonyl (–C–O). The peaks observed in the FTIR spectra show the diverse functional groups in the Prosopis juliflora root powder biomass. The peaks at 2884.76 cm^{-1} and 2945.96 cm^{-1} are caused by the carbon atoms in the (-CH) group and the -CHO (aldehyde) group. Moreover, a 1320–1000 cm^{-1} peak indicates C–O stretching, typically associated with alcohols and carboxylic acids. A significant finding in the FTIR spectra is the movement of peaks following the biosorption of metal ions (Laxmipriya et al., 2020). More precisely, the 3526.11, 3749.11, and 1771.76 cm^{-1} peaks shift to 3504.35, 3743.31, and 1773.71 cm^{-1}, respectively. This modification demonstrates how metal ions engage with and are taken in by the -OH and C-O groups (Long et al., 2021). The C-O stretching vibrations of alcohols and carboxylic acids are associated with the band originally found at 1314.74 cm^{-1}, which shifted to 1365.79 cm^{-1} after biosorption.
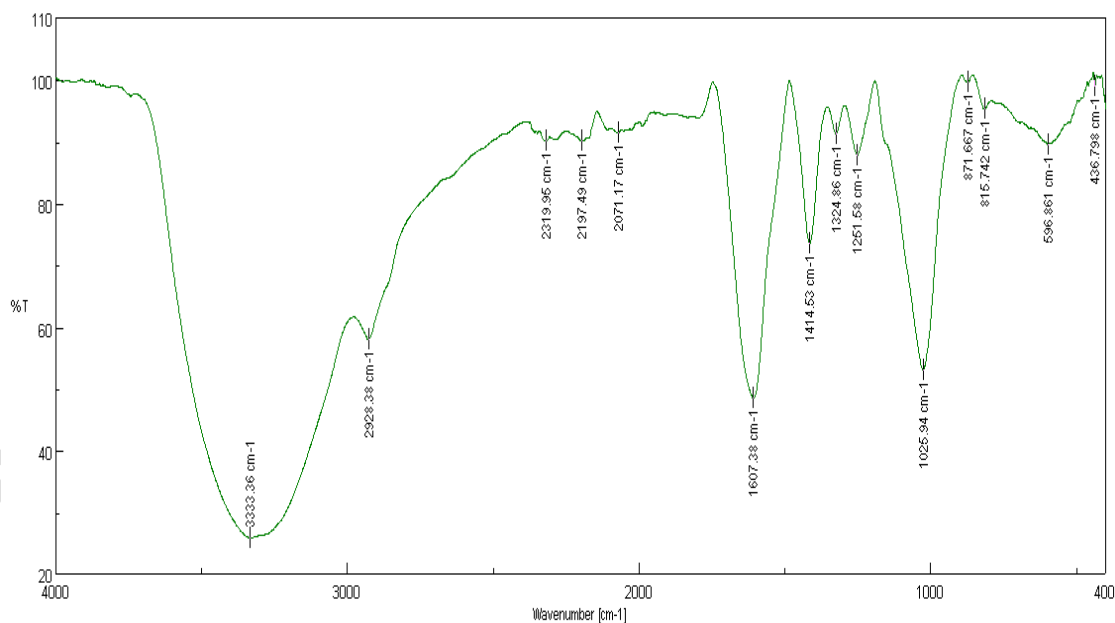

Figure 1 FTIR peaks of raw and dyes loaded adsorbent

3.2 Scanning Electron Microscope

SEM analysis is utilized to characterize the forms and surface area of the biosorbent. Images were captured with a scanning electron microscope (SEM) before and during biosorption. Figure 2(a) shows an SEM image of the biosorbent before biosorption. Figure 2(b) shows the biosorbent

containing absorbed CV, CR, and MB dyes. Scanning electron microscopy (SEM) allows for the generation of detailed images of the sample's surface, thoroughly examining the structural alterations in the material during biosorption. In Figure 2(a), the varied porous structure of the biosorbent is displayed. In Figure 2(b), the biosorbent exhibits a filamentous structure and a mix of porous structures. This finding may be related to the rough surface structure of the powder (Nyemaga et al., 2021). Analyzing the arrangement is essential in pinpointing possible binding sites for the target pollutants, just like in physical biosorption.

| (a) | (b) |
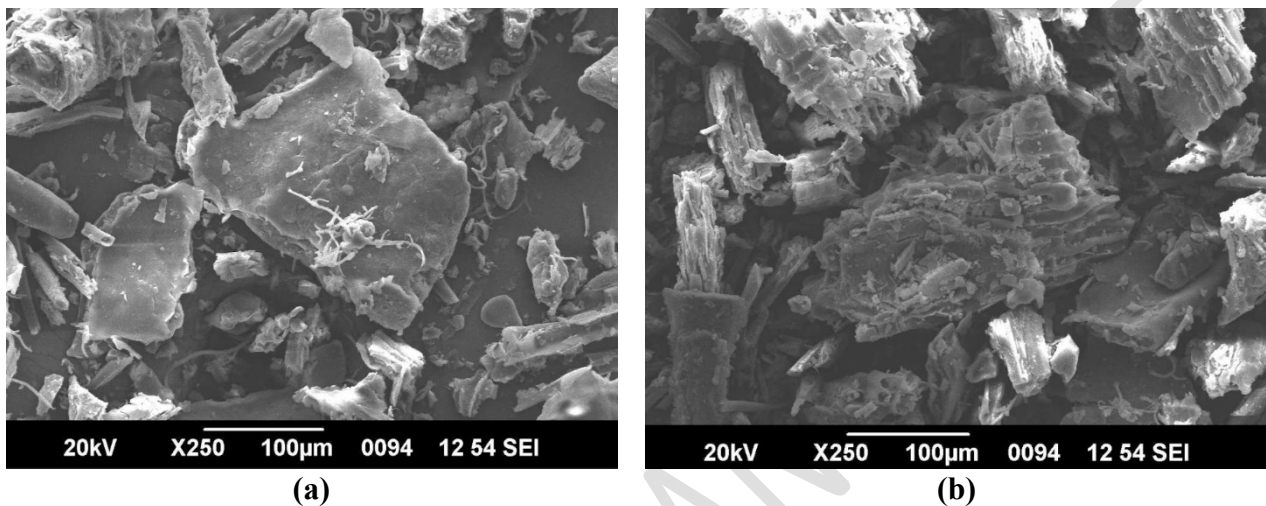
Figure 2 (a) Raw and (b) metal ions adsorbed PJRP biosorbent SEM image

3.3 Impact of pH

To enhance the effectiveness of the adsorption process, it is crucial to optimize the pH level. Understanding the connection between the ionization of functional groups, the adsorbate speciation, and the biosorbent's surface charge is essential for efficient contaminant removal. This study examined the effect of pH values ranging from 1.0 to 7.0 on the efficiency of azo dyes. The initial dye concentration of 20 mg/L, PJRP dose of 0.05 g/25 mL, equilibrium duration of 90 min at 25±1°C, and 200 rpm of constant stirring speed were adopted for this study. The azo dyes' adsorption rose when the pH rose in acidic environments, as seen in Fig. 3; however, further pH rise did not influence the adsorption process in alkaline solutions. The study found that increasing the pH from 2.0 to 6.0 directed a higher elimination of CV, CR, and MB dyes before the efficiency decreased. The competition among negatively charged H_3O^+ ions and positively charged azo dyes improved the efficiency of biosorption removal within the pH range of 2.0 to 6.0 (Pongthipun et al., 2021). However, the ability of biosorption decreased when hydroxide ions were added to CV, CR, and MB ions at pH 6.0. The study found that CV had a removal effectiveness of up to 88.02%, CR had 94.42%, and MB had 97.28% efficiency at a pH of 6.0.
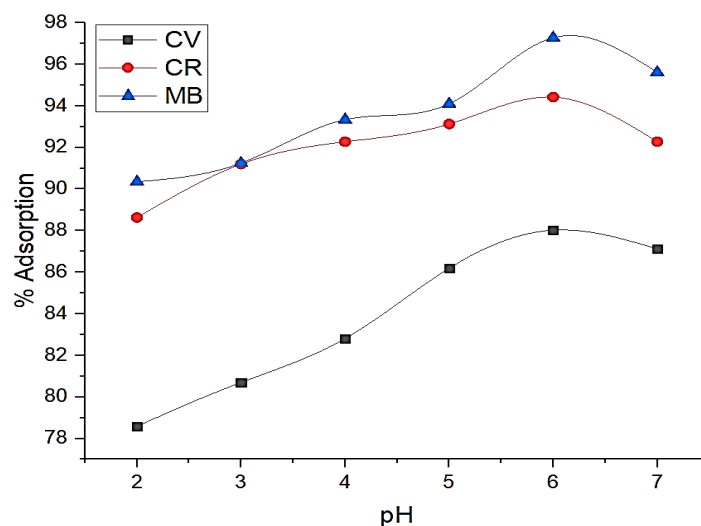
Figure 3 Impact of pH for the adsorption of the azo dyes using PJRP

3.4 Impact of PJRP dose

This study investigates the influence of varying quantities of biosorbent on the extraction of metal ions. Specifically, we incorporated 1 to 5 grams of biochar into synthetic solutions containing ten mg/L concentrations of azo dyes. Following prior research to establish the optimal pH, we adjusted the solution's pH accordingly. The mixture was agitated for 45 minutes at 25°C and 170 rpm. The findings (Fig. 4) show that the dyes were removed significantly with increased PJRP dose. According to the data, the maximum biosorption rates for CV of 81.48%, CR of 71.27%, and MB of 72.37% were achieved with a 4.0 g of biosorbent. There are more adsorption sites, which accounts for the rise in percentage removal when the adsorbent dose is increased. At increasing dosages of the adsorbent, the adsorption capacity was less. A larger adsorbent concentration brings this about, making more exchangeable sites or surface area available (Fatemeh et al., 2020).
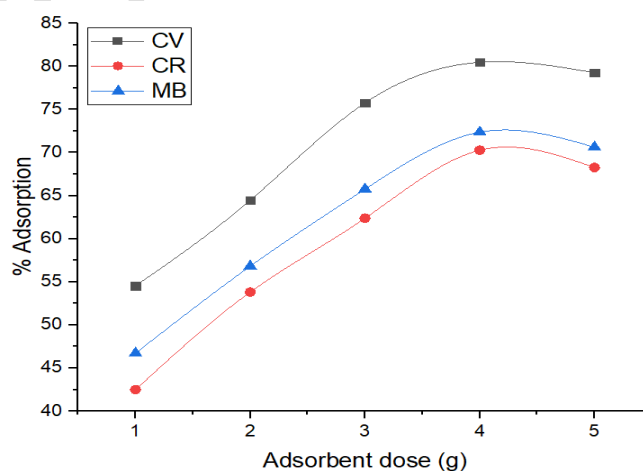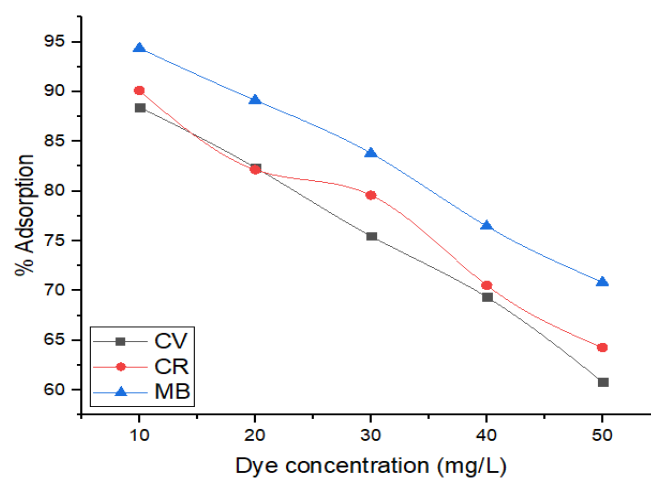

Figure 4 Impact of adsorption efficiency by altering the PJRP dose

## 3.5 Impact of Initial Dye Concentration

The concentrations were varied from 10 to 50 ppm, maintaining a pH of 6.0, using 4.0 grams of biosorbent, and allowing for a 45-minute interaction at room temperature. The capacity of biosorption (mg/g) over time at the optimal pH is shown in Figure 5. Because the adsorbents have a wide surface area accessible for the adsorption of the dye, both the potential for adsorption and the rate of % removal are initially higher. An increase in the concentration of dyes results in a decrease in adsorption efficiency and develops a concentration gradient. The increase in the concentration of dyes from 10 to 50 mg/L resulted in a reduction in adsorption capacity. The findings displayed in Fig. 5 demonstrate a decline in the elimination rates for CV (from 93.63% to 65.47%), CR (from 89.27% to 69.5%), and MB (from 82.39% to 70.28%). This decline happened due to the availability of more sites with lower initial azo dye levels (Hadj et al., 2015).

Figure 5 Impcat of adsorption efficiency by altering the azo dye concentration

3.6 Impact of Contact Time

The investigation analyzed the impact of varying the contact length between the biosorbent and azo dyes from 10 minutes to 1 hour on the outcomes shown in Figure 6. Initially, the removal of azo dyes happened quickly, however, subsequent stages did not exhibit significant variations. After 50 minutes, there was no further increase in the trapping of CV, CR, and MB as the uptake of azo dyes reached a plateau. This stabilization occurred when the surface of the adsorbent became saturated, resulting in repulsive forces that reduced the absorption of metal ions. Additionally, as time passed, the mass transfer from liquid to solid phases decreased because azo dye molecules had to move through densely packed pores over long distances, resulting in a lower adsorption efficiency (Muthaiyan & Rengasamy 2013).
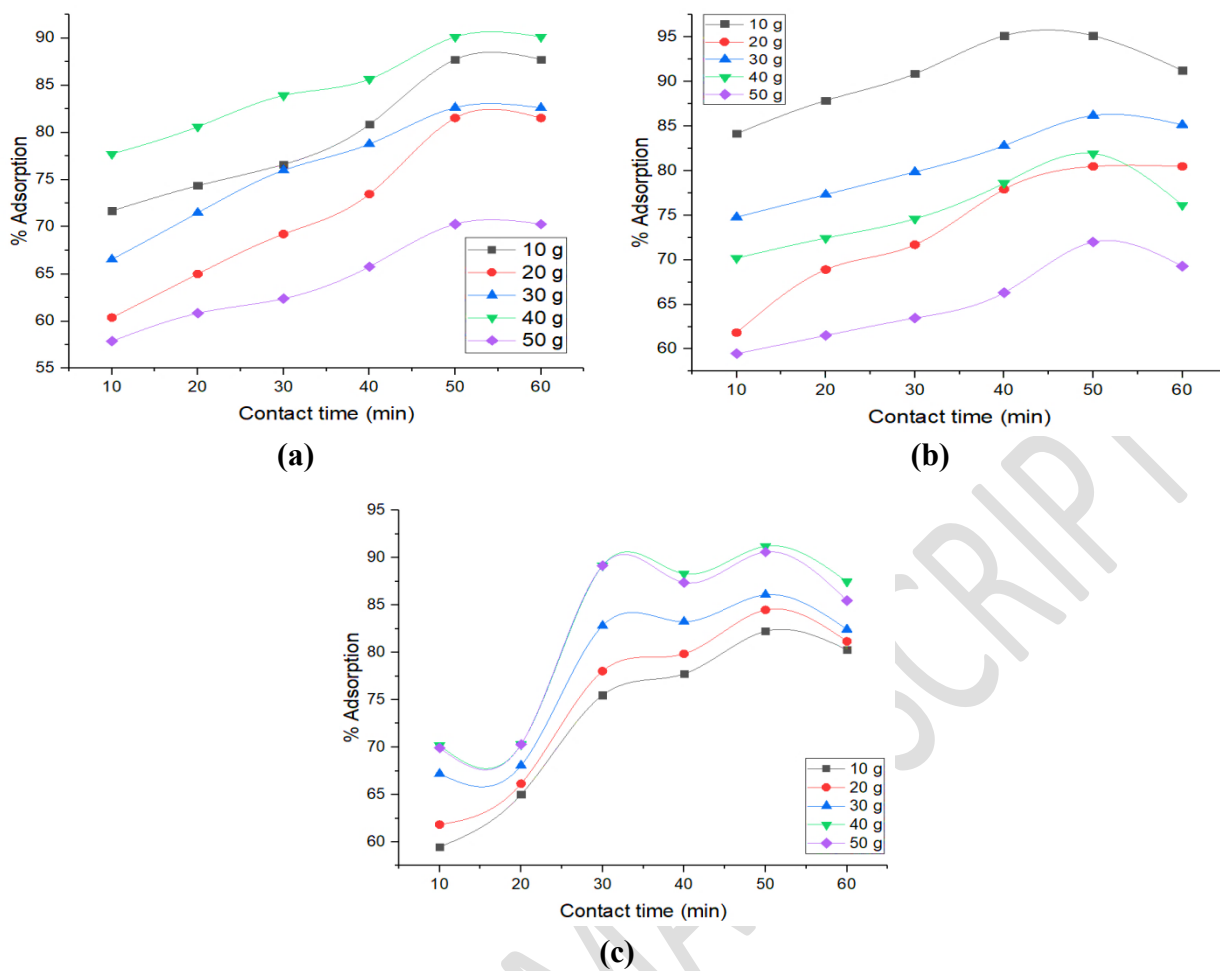
Figure 6 Effect of reaction time variation on adsorption efficiency for (a) CV, (b) CR, and (c) MB dyes

3.7 pH – ZPC

The pH$_{zpc}$ value of 4.54 for the PJRP biosorbent plays a pivotal role in determining its adsorption capabilities across different pH levels. Above this pH$_{zpc}$, the biosorbent's surface becomes negatively charged, promoting the adsorption of positively charged azo dyes. In contrast, under acidic conditions (below pH 4.54), the surface is positively charged, which can favour anion adsorption (Fig. 7). This explains why the PJRP biosorbent demonstrated optimal adsorption performance at basic pH levels, aligning with previous research. Understanding the pH$_{zpc}$ helps optimize the adsorption process for azo dyes in water treatment, ensuring better efficiency by tailoring the pH conditions to suit the interface among the biosorbent and the azo dyes (Wilson et al., 2020).
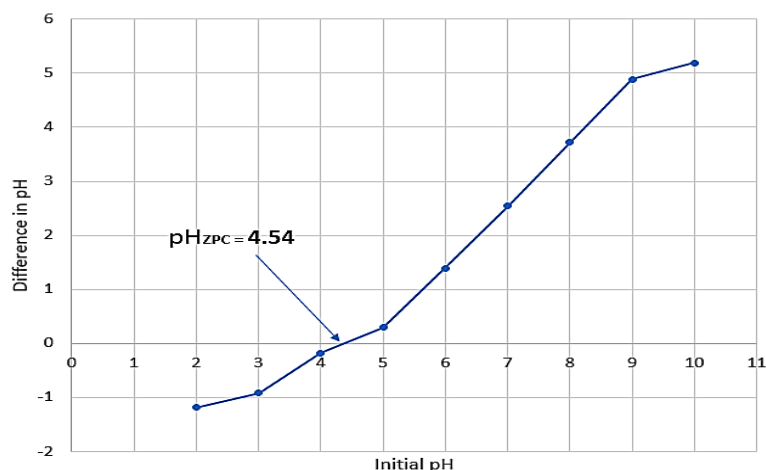
Figure 7 pH_ZPC of the batch adsorption studies

3.8 Isotherm studies

The isotherm in the adsorption process provides an insight into the diffusion of adsorption molecules within the liquid and solid phases as the process nears equilibrium (Nida et al., 2021). It is crucial to analyse the best model for the case under study by fitting the isotherm data to many isotherm models. The various isotherm models interpreted the adsorption of the azo dyes by PJRP across the complete range of concentrations investigated.
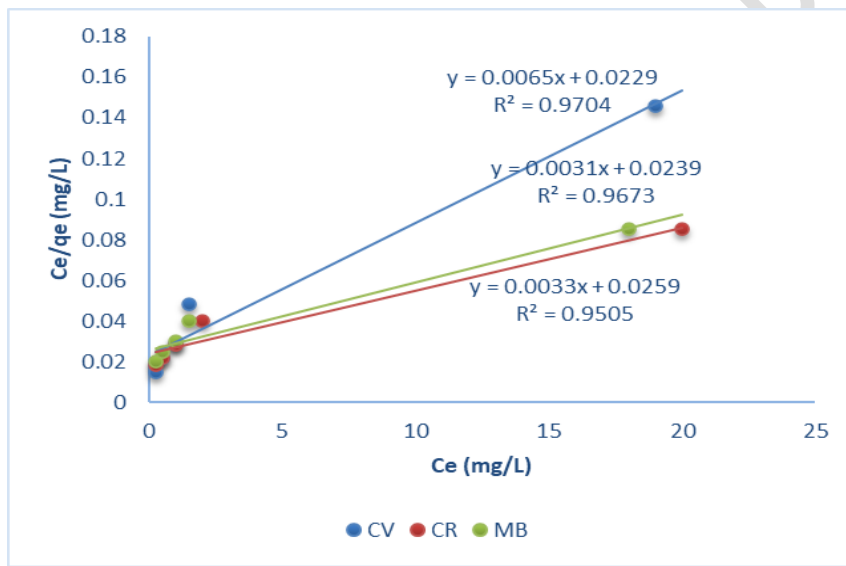
3.7.1 Langmuir isotherm

The Langmuir isotherm model posits that biosorption occurs as a monolayer on a consistent and uniform biosorbent surface (Radia et al., 2018). Equation 3 represents the linear form of this isotherm model:

$$\frac{C_e}{q_e} = \frac{1}{Q_o b} + \frac{C_e}{Q_o} \qquad (3)$$

The amount of adsorbate that is adsorbed per unit of adsorbent, expressed in milligrams per gram (mg/g), is represented by q_e. The equilibrium concentration of the dye is measured in milligrams per litre (mg/L), while the Langmuir constants Q_o and b indicate the adsorption capacity and the rate of adsorption, respectively. Straight lines with a slope of $1/Q_o$ were obtained for CR, CV, and MB when C_e/q_e was plotted vs C_e. The values of the Langmuir model are obtained and demonstrated in Figure 8. This chart shows a direct correlation between the levels of CV, CR, and MB dyes in the solution (mg/L) and the quantity of these ions absorbed by each unit mass (g) of PJRP. The outcome showed that CR, CV, and MB adsorption on PJRP follows the Langmuir isotherm and that dye molecules form a monolayer covering the outer surface of PJRP. Using this isotherm, the Langmuir constants b and Q_o were computed for CR, CV, and MB. Table 1 lists their results. The crucial features of the Langmuir isotherm can be conveyed through a dimensionless equilibrium parameter (R_L), as illustrated in the following equation 4:

$$R_L = \frac{1}{(1+bC_o)} \qquad (4)$$

The highest dye concentration, indicated as C_o (measured in mg/L), relates to the Langmuir constant, b. The R_L value can signify four distinct scenarios: linear ($R_L = 1$), unalterable ($R_L = 0$), positive ($0 < R_L < 1$), and negative ($R_L > 1$). Table 1 illustrates that the RL values for Pb, Cd, and Cu ions range between 0 and 1, affirming the adsorption method's efficacy. The concentration range examined yielded R_L values of 0.611 for CV, 0.612 for CR, and 0.165 for MB. These results confirmed that the PJRP enhanced the dyes CR, MB, and CV adsorption during the experimental procedure (Saeed et al., 2021). The elevated R^2 values demonstrate that the Langmuir model accurately reflects the equilibrium data, affirming its suitability for estimating the adsorption process.

Figure 8 Langmuir isotherm plot for azo dye adsorption using PJRP

3.7.2 Freundlich isotherm

This experiential study provides insight into biosorption on surfaces characterized by heterogeneity. It suggests that adsorption happens at sites with diverse energy levels, possibly leading to multilayer biosorption (Narges et al., 2018). Equation 5 represents the linear form of this isotherm model:

$$q_e = K_f \, C_e^{\frac{1}{n}} \qquad (5)$$

The K_f constant in the Freundlich isotherm [mg/g (L/mg)n] denotes the quantity of dye that is adsorbed onto the adsorbent, while the n constant indicates the intensity of the adsorption, thereby providing insight into the efficacy of the adsorption process. The Langmuir study shows higher correlation coefficients when comparing these two models, suggesting a stronger alignment with the adsorption data. Figure 9 represents the plot of ln q_e against ln $C_{e,\ which}$ was used to assess the applicability of the Freundlich model. This is followed by the adsorption of CR, CV, and MB, as

seen by the two dyes' straight lines in this illustration having a slope of "1/n." With a range of 0 to 1, the slope 1/n represents surface heterogeneity or adsorption intensity.

3.7.3. Temkin isotherm

A linearized version of the Temkin isotherm is provided in Equation 6.

$$q_{eq} = \frac{RT}{b}\ln K_T + \frac{RT}{b}\ln C_e \qquad (6)$$

Where T indicates the absolute temperature in Kelvin (K), R is the general gas constant, quantified as 8.314 J/mol K, A is the constant of this model expressed in litres per gram (L/g), and b is the heat adsorption, given in joules per mole (J/mol). The linear plot of ln C_e against q_e might be used to compute b and A (Fig. 10). According to this isotherm, the adsorbent-adsorbate interaction causes the heat of adsorption of every molecule in the layer to drop linearly with attention.
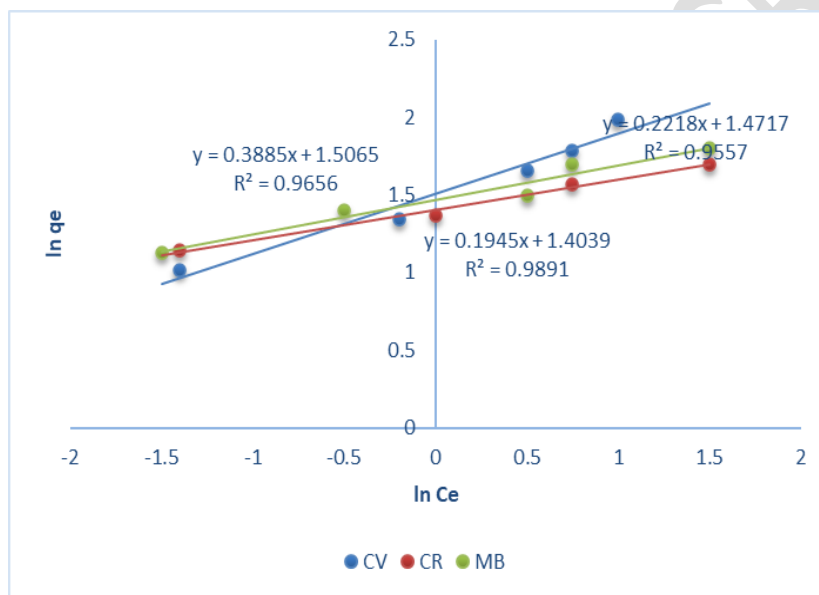
Figure 9 Freundlich isotherm plot for azo dye adsorption using PJRP

Additionally, it assumes that binding energies are uniformly distributed during adsorption up to a certain maximum value. In contrast to the other models, the Freundlich model matched the data acquired for the Langmuir, Temkin, and Freundlich isotherms at the various concentrations under investigation. The Freundlich model better describes the biosorbent's saturation behaviour than the Langmuir and Temkin models. This suggests that, given the experimental setup, heterogeneous surface conditions occur. The differences in adsorption capacities and affinities among various adsorbents can be largely attributed to differences in their physico-chemical properties (Michal et al., 2022). Additionally, variations in experimental conditions, including pH, temperature, and contact time, can greatly impact adsorption outcomes. Consequently, even minor differences in these conditions can lead to variations in the adsorption performance observed across different studies and adsorbent materials.
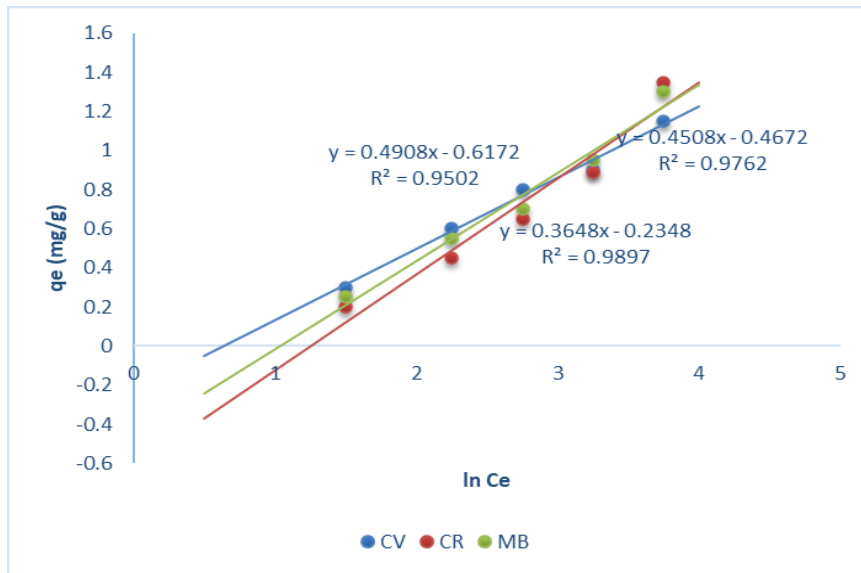
Figure 10 Temkin isotherm plot for azo dye adsorption using PJRP

**Table 1 Constants of isotherm studies for the adsorption of azo dyes using PJRP**

Isotherm Model	Types of metal ions			
	Parameters	CV	CR	MB
Langmuir	q_{max} (mg/g)	9.037	9.128	8.923
	R_L (L/mg)	0.228	0.261	0.205
	R^2	0.9704	0.9505	0.9673
Freundlich	K_f ((mg/g) (L/mg)$^{1/n}$)	2.729	1.951	1.657
	n (g/L)	2.854	2.253	1.928
	R^2	0.9656	0.9557	0.9891
Temkin	K_T (L/mol)	1.31×10^6	1.15×10^4	1.91×10^4
	b x 10^{-6} (Jg/mol^2)	25.4	12.4	27.1
	R^2	0.9897	0.9502	0.9762

3.8 Adsorption kinetics

As elucidated by a study of adsorption kinetics, the solute uptake rate determines the time that adsorbates reside at the solid/solution interface. The research utilized the first and second pseudo-kinetic models to assess CR, CV, and MB adsorption kinetics on the PJRP. The pseudo-first-order linear equation is expressed as follows (Eqn. 7):

$$\log(q_e - q) = \log q_e - \frac{k}{2.303}t \qquad (7)$$

Figuring out a linear relationship between log (q_e−q_t) and t (Fig. 11) will allow one to use the slope and intercept of the plot to compute k_1 and q_e, respectively. The adsorption process's whole range was not well-fitted by the first-order Lagergren equation, which was only typically valid during the first phase of the contract period, as indicated by the lines' form (Nathalia et al., 2021).
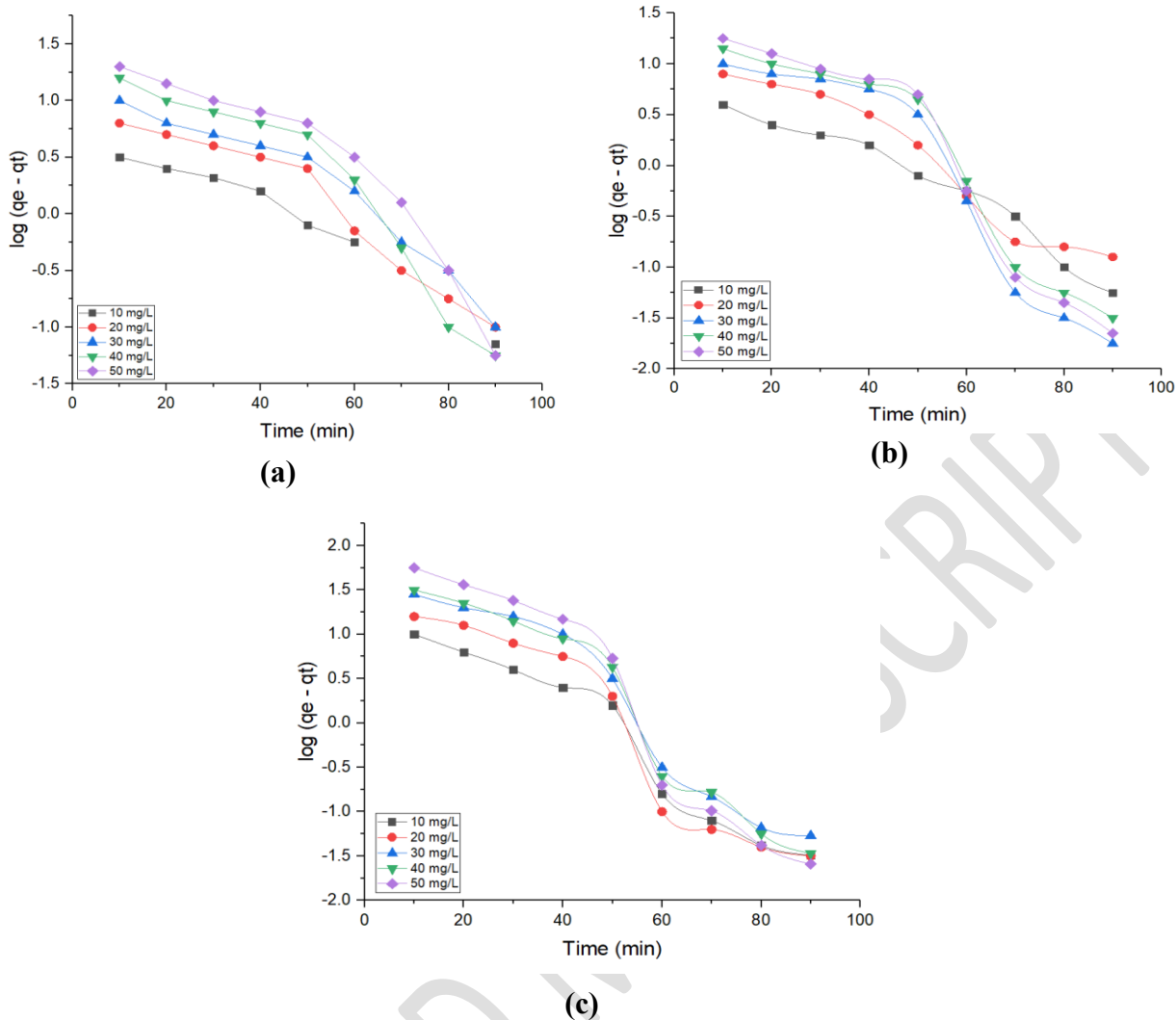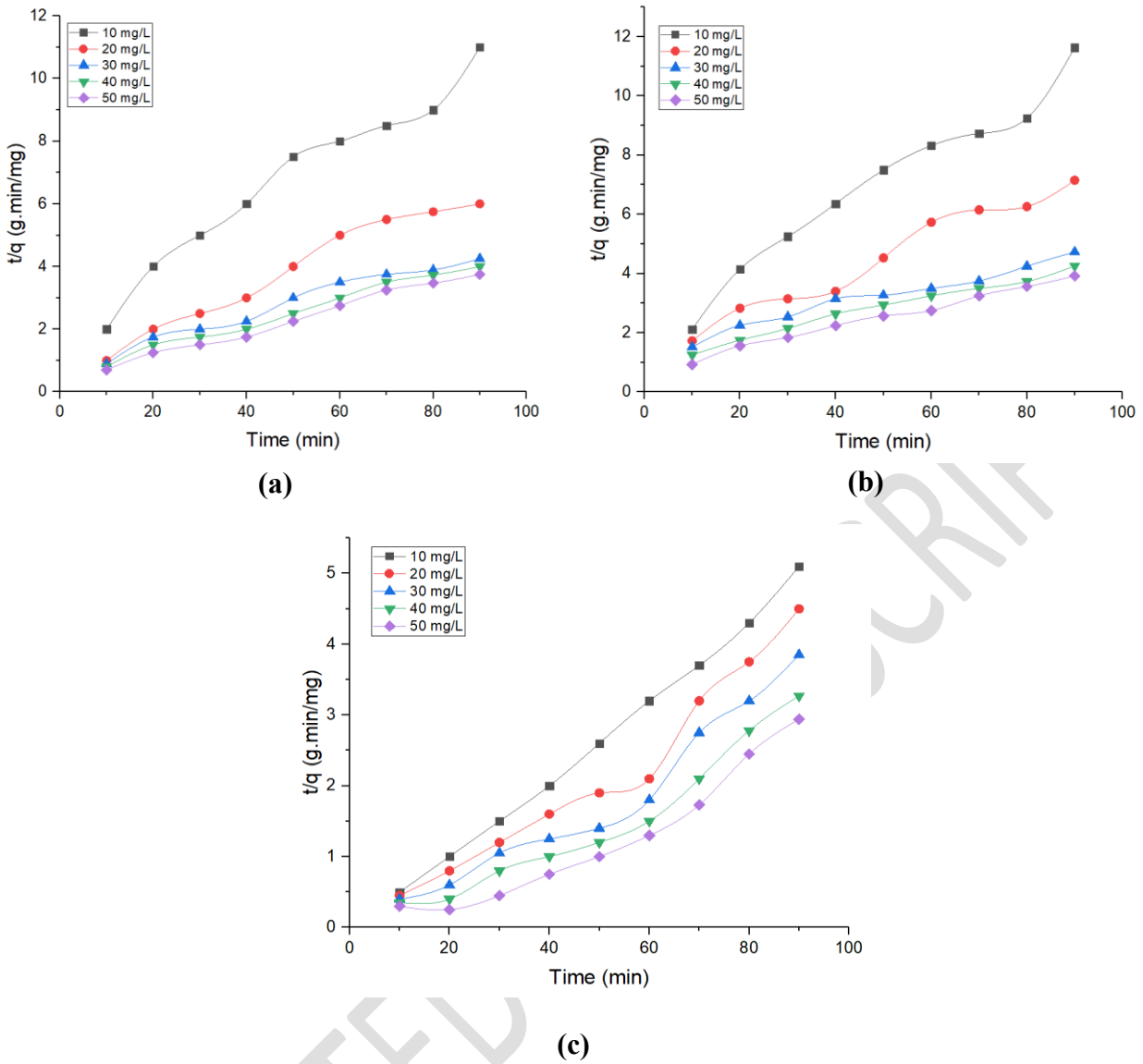
Figure 11 Pseudo-first-order kinetic plots for (a) CR, (b) CV, and (c) MB dyes adsorption

The linear equation of this kinetic equation is represented as:

$$\frac{t}{q_t} = \frac{1}{k_2 q_e^2} + \frac{t}{q_e} \qquad (8)$$

Plotting t/q_t against t (Fig. 12) produces excellent straight lines at varying CR, CV, and MB starting concentrations. The findings illustrated in Table 2 pertain to the fitting of experimental data for CR, CV, and MB adsorption on PJRP, employing the pseudo-first-order and pseudo-second-order models. The second-order pseudo-type model offers a more precise representation, as reflected by its correlation coefficients (R^2), which are consistently higher than those of the first-order model, with a minimum value of 0.99. Additionally, there is a strong integration between the computed q_e readings and the experimental results. Based on these findings, the adsorption system under study fits into the second-order pseudo-kinetic model. The Boyd kinetic model is applied to ascertain the rate-controlling step in the biosorption process, specifically distinguishing between film diffusion and intraparticle diffusion.

Figure 12 Pseudo-Second -order kinetic plots for (a) CR, (b) CV, and (c) MB dyes adsorption

Equation 9 represents the linear form of this kinetic model.

$$B_t = -0.4977 - \ln(1 - F) \qquad (9)$$

The Boyd function, denoted as Bt at time 't,' is utilized with the fractional adsorption F, which can be calculated using the formula F = q_t/q_e. This model is instrumental in determining the dominant diffusion mechanism within the biosorption process. The "Bt versus t" graph is critical for analyzing the linearity of the experimental results. The slowest step of the adsorption process due to intra-particle diffusion confirms the linear relationship produced from the origin (Ahmed et al., 2022). Conversely, the adsorption of metal ions by PJRP influenced by external or film diffusion confirms the linear plots do not intersect the origin. Figures 13 present the plots corresponding to different concentrations of azo dyes on PRJP. The calculated values of D_i and B from these plots are detailed in Table 1, along with the regression coefficient R^2.
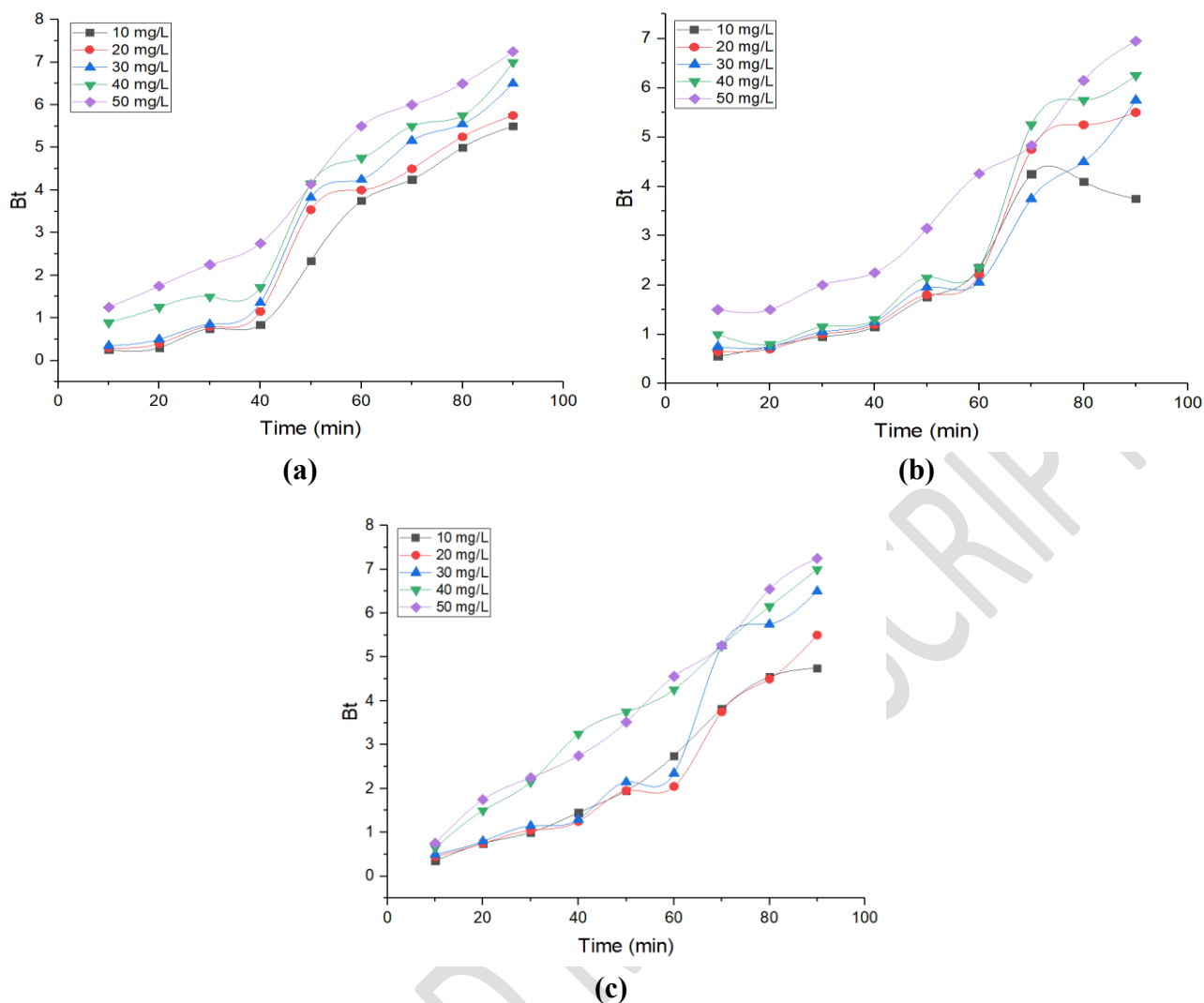
Figure 13 Boyd kinetic plots for (a) CR, (b) CV, and (c) MB dyes adsorption

3.9 Thermodynamic parameters

The rise in adsorption as the temperature rises indicates an endothermic process that may be thermodynamically described by calculating quantities like change in free energy, enthalpy, and entropy ($\Delta G°$, $\Delta H°$, and $\Delta S°$). The following equations 10 and 11 were used to determine these parameters:

$$\Delta G^o = -RT \ln K_L \qquad (10)$$

$$\ln K_L = -\frac{\Delta G^o}{RT} = -\frac{\Delta H^o}{RT} + \frac{\Delta S^o}{RT} \qquad (11)$$

Table 2 Kinetic constants of metal ion adsorption process using Prosopis juliflora roots

| S. No.	Nature of the metal ion	Concentration of the ion solution (mg/L)	Pseudo First Order			Pseudo Second Order					Boyd		
			k (min^{-1})	q_e, cal (mg/g)	R^2	K (g/mg.min) X 10^{-3}	q_e, cal (mg/g)	h (mg/g.min)	q_e, exp (mg/g)	R^2	B	D_i (x 10^{-3}m^2/s)	R^2
1.	CV	10	0.0668	11.492	0.918	8.980	13.988	1.751	12.983	0.997	0.086	11.942	0.918
2.		20	0.0736	28.504	0.921	4.722	26.878	3.607	25.126	0.997	0.074	12.605	0.912
3.		30	0.0760	46.559	0.927	2.826	41.766	3.986	38.214	0.996	0.076	12.848	0.928
4.		40	0.0829	83.716	0.946	1.969	56.552	4.552	50.873	0.995	0.083	14.207	0.944
5.		50	0.0714	84.139	0.936	1.353	66.763	4.793	59.129	0.994	0.085	14.762	0.938
1.	CR	10	0.0678	12.445	0.927	7.763	13.968	1.522	12.840	0.997	0.068	11.492	0.928
2.		20	0.0714	29.040	0.911	3.600	26.513	2.778	24.450	0.997	0.072	12.373	0.914
3.		30	0.0737	54.935	0.928	2.870	38.642	3.623	36.892	0.979	0.086	14.354	0.925
4.		40	0.0875	84.121	0.924	1.530	51.235	4.617	48.711	0.969	0.088	14.730	0.927
5.		50	0.0921	94.189	0.931	0.949	62.458	4.655	59.122	0.994	0.093	15.177	0.931
1.	MB	10	0.0645	11.561	0.916	8.186	13.514	1.495	12.631	0.975	0.066	10.895	0.912
2.		20	0.0737	30.794	0.922	4.250	25.641	2.466	24.221	0.976	0.072	12.605	0.922
3.		30	0.0898	69.343	0.935	2.522	37.307	3.640	35.015	0.964	0.090	15.120	0.936
4.		40	0.0806	74.989	0.930	1.478	52.363	4.908	47,234	0.965	0.083	14.782	0.930
5.		50	0.0875	92.336	0.935	1.258	66.672	5.392	59.286	0.972	0.088	13.520	0.935

K_L and Q_ob, the adsorption process's equilibrium constant (L/mg), are the same. The temperature, in absolute terms, is denoted by T. The gas constant by R. If ln K_L is plotted as a function of 1/T, an annular line (R^2= 0.998 for MB, 0.994 for CR and 0.992 for CV) is obtained (Fig. 14). It was possible to evaluate ΔH° and ΔS° from the intercept and slope, respectively. A comprehensive summary of the thermodynamic constants, including the variations in ΔS°, ΔH°, and ΔG°, is provided in Table 3.

The study applied recognized methodologies to derive these values. The results demonstrate that as the temperature rises, free energy consistently declines, representing that the adsorption of azo dyes is both impulsive and more promising at higher temperatures. The positive enthalpy changes indicate that the biosorption process is endothermic, with heat absorption playing a role in improving reaction efficiency. Additionally, the positive change in entropy suggests an increase in disorder at the solid-liquid boundary, highlighting the effectiveness of the biosorption process under the conditions studied.

(a)

(b)

(c)
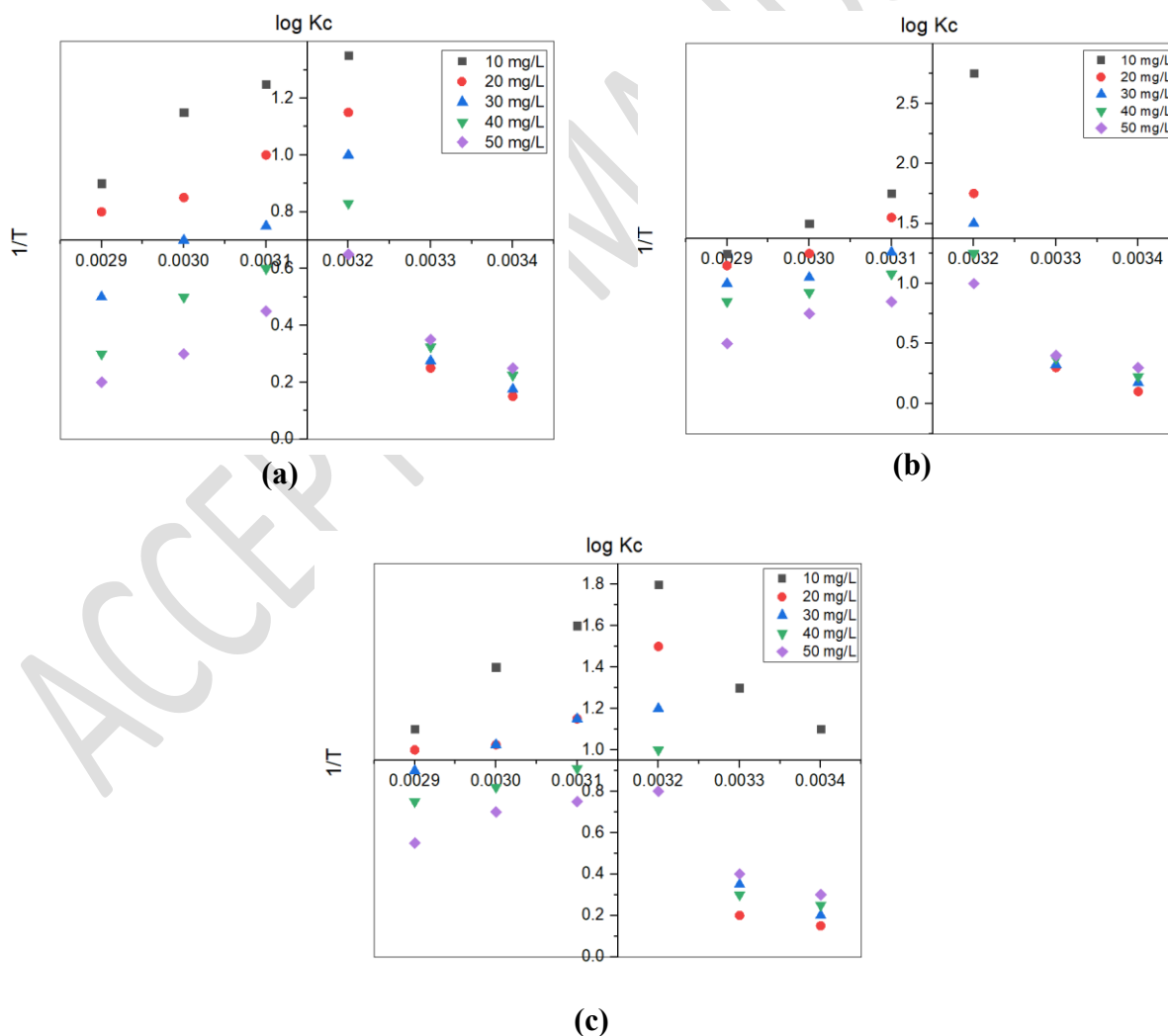
Figure 14 Thermodynamic plots for (a) CR, (b) CV, and (c) MB dyes using PJRP

Table 3 Thermodynamic constants of the azo dye adsorption using PJRP

CV dye concentration	ΔH° (KJ/mol)	ΔS° (J/mol/	ΔG° (kJ/mol)			
			15°C	30°C	45°C	60°C
10	-71.28	192.46	-11.46	-9.71	-8.26	-7.42
20	-39.57	88.71	-9.72	-7.41	-7.12	-6.29
30	-21.29	59.72	-6.16	-5.35	-5.08	-4.92
40	-15.19	39.97	-4.57	-3.16	-3.01	-2.91
50	-11.72	29.27	-2.72	-2.19	-2.01	-1.82
CR dye concentration						
10	-62.46	151.49	-15.49	-13.48	-9.72	-8.24
20	-47.19	86.71	-10.22	-9.64	-8.67	-7.49
30	-32.42	61.16	-9.18	-8.15	-7.27	-6.72
40	-21.13	42.27	-8.47	-7.29	-6.73	-5.49
50	-17.28	25.72	-7.21	-6.46	-5.19	-4.18
MB dye concentration						
10	-40.02	99.09	-11.16	-9.29	-8.54	-7.31
20	-25.45	51.27	-9.01	-7.89	-7.02	-6.02
30	-19.92	40.51	-7.69	-6.32	-5.93	-5.29
40	-15.56	31.48	-6.24	-5.89	-5.05	-4.78
50	-13.29	28.92	-5.92	-5.02	-4.58	-4.22

3.10 Batch desorption study

The efficiency of removing dyes from spent adsorbent (PJRP) depends greatly on how well the desorption process works. The data in Table 4 illustrates different levels of sulfuric acid concentrations used in a batch desorption test, ranging from 0.1 to 0.4 N. The findings indicate that increased levels of sulfuric acid resulted in improved recovery of azo dyes. After treatment with 0.3 N H_2SO_4, the recovery rate remained stable and reached its highest point for recovery. However, higher levels of H_2SO_4 did not lead to any further increase in recovery rates (Chuanbin et al., 2022). Therefore, it was concluded that a concentration of 0.3 N H_2SO_4 is most effective for extracting azo dyes from the recycled PJRP. In addition, the PJRP was successfully restored and utilized again as an adsorbent in subsequent studies.

Table 4 Desorption studies of azo dyes using sulfuric acid

Initial concentration (10 mg/L)	Efficiency of dye removal (%)	Concentration of H$_2$SO$_4$			
		0.10 N	0.20 N	0.30 N	0.40 N
		% Desorption of azo dyes			
CV	94.92	79.28	82.67	88.59	84.73
CR	89.73	67.51	72.29	79.67	73.82
MB	90.28	69.59	75.54	80.59	76.13

4. CONCLUSION

The Prosopis juliflora root powder exhibited a significant capacity for dye adsorption, with its efficiency being affected by variables such as pH, dye concentration, contact duration, and the amount of adsorbent used. The process was more efficient in acidic to neutral pH environments, where the interplay between the adsorbent's surface charge and the dye molecules' ionic state was crucial to the adsorption mechanism. The adsorption kinetics conformed to pseudo-second and first-order behaviour, suggesting that chemisorption is the dominant process. Furthermore, the Langmuir and Freundlich models most accurately represented the adsorption isotherms, indicating the occurrence of multilayer adsorption on a heterogeneous surface. Utilizing Prosopis juliflora roots, readily available and sustainable biomass, offers an eco-friendly solution for managing wastewater contamination by azo dyes, contributing to cleaner water resources. Prosopis juliflora root powder provides a cost-effective, sustainable adsorbent with the potential for large-scale application in dye wastewater treatment.

REFERENCES

Priya A.K, V. Yogeshwaran, Saravanan Rajendran, Tuan K.A. Hoang, Matias Soto-Moscoso, Ayman A. Ghfar and Chinna Bathula (2022). Investigation of the mechanism of heavy metals (Cr^{6+}, Pb$_{2+}$& Zn^{2+}) adsorption from aqueous medium using rice husk ash: Kinetic and thermodynamic approach, Chemosphere, 286, 131796. https://doi.org/10.1016/j.chemosphere.2021.131796

Abdelmajid Regti, My Rachid Laamari, Salah-Eddine Stiriba and Mohammadine El Haddad (2017). The potential use of activated carbon prepared from Ziziphus species for removing dyes from wastewaters. Applied Water Science, 7, 4099 – 4108. https://doi.org/10.1007/s13201-017-0567-8

Achmad Syafiuddin, Salmiati Salmiati, Jonbi Jonbi and Mohamad Ali Fulazzaky (2018). Application of the kinetic and isotherm models for better understanding of the behaviors of

silver nanoparticles adsorption onto different adsorbents, Journal of Environmental Management, 15, 59 -70. https://doi.org/10.1016/j.jenvman.2018.03.066

Ahmed Eleryan, Uyiosa O. Aigbe, Kingsley E. Ukhurebor, Robert B. Onyancha, Tarek M. Eldeeb, Mohamed A. El-Nemr, Mohamed A. Hassaan, Safaa Ragab, Otolorin A. Osibote, Heri S. Kusuma, Handoko Darmokoesoemo and Ahmed El Nemr (2022). Copper(II) ion removal by chemically and physically modified sawdust biochar. Biomass Conversion and Biorefinery. https://doi.org/10.1007/s13399-022-02918-y

Candelaria Tejada-Tovar, Ángel Villabona-Ortíz and Ángel Darío Gonzalez-Delgado (2021). Adsorption of Azo-Anionic Dyes in a Solution Using Modified Coconut (Cocos nucifera) Mesocarp: Kinetic and Equilibrium Study, Water, 13, 1382. https://doi.org/10.3390/w13101382

Chuanbin Wang, Xutong Wang, Ning Li, Junyu Tao 2, Beibei Yan, Xiaoqiang Cui and Guanyi Chen (2022). Adsorption of Lead from Aqueous Solution by Biochar: A Review. Clean Technologies, 4, 629 – 652. https://doi.org/10.3390/cleantechnol4030039

Fatemeh Elmi, Farshid Mohammadi Damghani, and Mojtaba Shokrollahzadeh Taleshi (2020). Kinetic and Isotherm Studies of Adsorption of the Metribuzin Herbicide on an Fe$_3$O$_4$/CNT@PDA Hybrid Magnetic Nanocomposite in Wastewater, Industrial and Engineering Chemistry Research, 59 (20), 9604 – 9610. https://doi.org/10.1021/acs.iecr.9b07077

Hadj Daoud Bouras, Oumessaâd Benturki, Noureddine Bouras, Mouloud Attou, André Donnot, André Merlin, Fatima Addoun and Michael D. Holtz (2015). The use of an agricultural waste material from Ziziphus jujuba as a novel adsorbent for humic acid removal from aqueous solutions. Journal of Molecular Liquids, 211, 1039 – 1046. Doi: https://doi.org/10.1016/j.molliq.2015.08.028

Laxmipriya Panda, Sandeep K. Jena, Swagat S. Rath and Pramila K. Misra (2020). Heavy metal removal from water by adsorption using a low-cost geopolymer, Environmental Science and Pollution Research, 27, 24284 – 24298. https://doi.org/10.1007/s11356-020-08482-0

Long Su, Haibo Zhang, Kokyo Oh, Na Liu, Yuan Luo, Hongyan Cheng, Guosheng Zhang and Xiaofang He (2021). Activated biochar derived from spent Auricularia auricula substrate for the efficient adsorption of cationic azo dyes from single and binary adsorptive systems, Water Science & Technology, 84 (1), 101 – 121. https://doi.org/10.2166/wst.2021.222

Mehrnaz Hosseinzehi, Masoumeh Khatebasreh and Arash Dalvand (2020). Modeling of Reactive Black 5 azo dye adsorption from aqueous solution on activated carbon prepared from poplar sawdust using response surface methodology, International Journal of Environmental Analytical Chemistry,18. https://doi.org/10.1080/03067319.2020.1819991

Michal Marciniak, Joanna Goscianska, Małgorzata Norman, Teofil Jesionowski, Aleksandra Bazan-Wozniak and Robert Pietrzak (2022). Equilibrium, Kinetic, and Thermodynamic Studies on Adsorption of Rhodamine B from Aqueous Solutions Using Oxidized Mesoporous Carbons, Materials, 15, 5773. https://doi.org/10.3390/ma15165573

Mohammed Benjelloun, Youssef Miyah, Gulsun Akdemir Evrendilek, Farid Zerrouq Sanae Lairini (2021). Recent Advances in Adsorption Kinetic Models: Their Application to Dye Types, Arabian Journal of Chemistry, 14 (4), 103031. https://doi.org/10.1016/j.arabjc.2021.103031

Muthaiyan Kumar and Rengasamy Tamilarasan (2013). Kinetics and Equilibrium Studies on the Removal of Victoria Blue Using Prosopis juliflora-Modified Carbon/Zn/Alginate Polymer Composite Beads, Journal of Chemical & Engineering Data, 58, 517 – 527. dx.doi.org/10.1021/je3012309

Narges samadani langeroodi, Zhaleh farhadravesh, Aliakbar dehno khalaji (2018) Optimization of adsorption parameters for Fe (III) ions removal from aqueous solutions by transition metal oxide nanocomposite. Green chemistry letters and reviews 11 (4): 404 – 413. Doi: https://doi.org/10.1080/17518253.2018.1526329

Nathalia Krummenauer Haro, Ivone Vanessa Jurado Dávila, Keila Guerra Pacheco Nunes, Marcela Andrea Espina de Franco, Nilson Romeu Marcilio and Liliana Amaral Féris (2021). Kinetic, equilibrium and thermodynamic studies of the adsorption of paracetamol in activated carbon in batch model and fixed-bed column, 11 (38). https://doi.org/10.1007/s13201-020-01346-5

Nida Fakhar, Suhail Ayoub Khan, Weqar Ahmad Siddiqi and Tabrez Alam Khan (2021). Ziziphus jujube waste-derived biomass as cost-effective adsorbent for the sequestration of Cd^{2+} from aqueous solution: Isotherm and kinetics studies. Environmental Nanotechnology, Monitoring & Management, 16, 100570. Doi: https://doi.org/10.1016/j.enmm.2021.100570

Nyemaga Malima, Shesan John Owonubi, E. H. Lugwisha and A. S. Mwakaboko (2021). Thermodynamic, isothermal and kinetic studies of heavy metals adsorption by chemically modified Tanzanian Malangali kaolin clay. International Journal of Environmental Science and Technology, 18 (10), 1-16. http://dx.doi.org/10.1007/s13762-020-03078-0

Pongthipun Phuengphai, Thapanee Singjanusong, Napaporn Kheangkhun and Amnuay Wattanakornsiri (2021). Removal of copper (II) from aqueous solution using chemically modified fruit peels as efficient low-cost biosorbents, Water Science and Engineering, 14 (4), 286 – 294. http://dx.doi.org/10.1016/j.wse.2021.08.003

Radia Labied, OumessaadBenturki, Adh' Ya Eddine Hamitouche and André´ Donnot (2018). Adsorption of hexavalent chromium by activated carbon obtained from a waste lignocellulosic material (Ziziphus jujuba cores): Kinetic, equilibrium, and thermodynamic

study. Adsorption Science and Technology, 36 (3-4), 1066-1099. Doi:10.1177/0263617417750739

Saeed Ullah Jan, Aziz Ahmad, Adnan Ali Khan, Saad Melhi, Iftikhar Ahmad, Guohua Sun, Cheng-Meng Chen and Rashid Ahmad (2021). Removal of azo dye from aqueous solution by a low-cost activated carbon prepared from coal: adsorption kinetics, isotherms study, and DFT simulation, Environmental Science and Pollution Research, 28, 10234 – 10247. https://doi.org/10.1007/s11356-020-11344-4

Wilson Mwandira, Kazunori Nakashima, Satoru Kawasaki, Allison Arabelo, Kawawa Banda, Imasiku Nyambe, Meki Chirwa, Mayumi Ito, Tsutomu Sato, Toshifumi Igarashi, Hokuto Nakata, Shouta Nakayama and Mayumi Ishizuka (2020). Biosorption of Pb (II) and Zn (II) from aqueous solution by Oceanobacillus profundus isolated from an abandoned mine, Scientific Reports, 10, 21189. https://doi.org/10.1038/s41598-020-78187-4